Natural Convection in a Porous Cavity with a Varying-Amplitude Wavy Wall Under a Partially Applied Magnetic Field: A Finite Element Study

Md. Motiur Rahman
Department of Mechanical Engineering, International University of Business Agriculture and Technology, Dhaka 1230, Bangladesh
*Correspondence: bari.rahman97@gmail.com

ABSTRACT

This study investigates natural convection within a square porous cavity subjected to a partially applied horizontal magnetic field along a section of the left vertical wall. The top and bottom horizontal walls are thermally insulated. The left wall is maintained at a high temperature, while the opposing right wall, characterized by a varying-amplitude wavy surface, is kept at a lower temperature. The Brinkman–Forchheimer-extended Darcy model is employed to simulate the fluid flow within the porous medium. The governing equations are numerically solved using the Galerkin finite element method, and the accuracy of the approach is validated through comparison with previous study. The effects of key parameters including the magnetic field length, Hartmann number, Rayleigh number, Darcy number, and the wall wave damping effect are analyzed in terms of streamlines, isotherms, and average Nusselt number. The results demonstrate that the magnetic field suppresses convective flow and reduces heat transfer, highlighting its potential for controlling thermal transport and fluid motion within porous enclosures. Furthermore, increasing the damping effect of wall waves reduces heat transfer by simplifying convective patterns.

Key Words: Partial magnetic field, Natural convection, Porous medium, Non-uniformly wavy cavity

1. INTRODUCTION

Natural convection plays a critical role in a wide range of engineering and industrial applications, including thermal regulation in electronic devices, passive cooling in building envelopes, solar energy systems, and thermal insulation in nuclear reactors (Pandey et al., 2019; Rahimi et al., 2019). Accurate prediction and control of fluid flow and heat transfer behavior are essential for optimizing the performance of such systems, especially when dealing with complex boundary conditions and external forces. In particular, porous enclosures have received growing attention due to their applications in geothermal energy extraction, packed bed reactors, and phase-change thermal storage systems (Parmar et al., 2023; Rath & Anita, 2023). The magnetic field is an important factor for controlling heat transfer and fluid flow, and it is commonly used to optimize efficiency across different thermodynamic systems as given in the literature (Davidson, 2001; Wu et al., 2015).

Recent investigations have further refined understanding of how magnetic fields, geometry, porous media, and nanofluid properties interact to affect heat transfer, flow structure, and entropy generation in natural convective systems. Tuli et al. (2023) studied non-Newtonian ferrofluid natural convection in a square cavity housing a heated wavy cylinder, finding that as the Hartmann number increases, flow is more suppressed and both average Nusselt number and entropy generation decrease; also, the power-law index and wave number significantly influence thermal boundary layer thickness. Kolsi et al. (2024) considered a hybrid nanofluid in an inclined porous cavity with a cross-shaped obstacle, under radiation and internal heat generation; they showed that increased porosity, reduced obstacle size, and larger heated wall surfaces improve heat transfer, while heat generation and stronger magnetic fields tend to reduce convective efficiency. Hasan et al. (2024) examined MHD convection with Joule (resistive) heating and internal heat generation in a two-layer chamber partially filled with porous medium, with both straight and wavy interfaces; they reported that thinner porous layers, lower corrugation amplitudes, and lower interface frequencies enhance Nusselt number, while increasing magnetic field strength reduces it. Finally, Halder et al. (2024) looked at MHD nanofluidic mixed convection in a butterfly-shaped cavity; they found that cavity shape, Hartmann number, and nanoparticle loading strongly affect both heat transfer and entropy generation, with certain geometries yielding significantly better thermal performance. Barman & Rao (2024) considered non-equilibrium local thermal non-equilibrium

(LTNE) free convection in a Darcy porous cavity with a wavy cold side wall, heated left wall, insulated top and bottom, and used the Galerkin finite element method to solve the governing equations. They evaluated how waviness (amplitude and number of undulations), Rayleigh-Darcy number, porosity, and interface heat transfer parameter affect temperature fields and Nusselt numbers. The results show that increasing waviness improves heat transfer for both fluid and solid phases. Geridonmez and Oztop (2020) along with their earlier related works (Geridonmez & Oztop, 2019; Geridonmez & Oztop, 2020b) conducted a mathematical investigation of natural convection in a square cavity subjected to a constant magnetic field. Using the radial basis function (RBF) method for spatial discretization and the backward Euler method for time integration, they solved the dimensionless governing equations. Their results indicated that the presence of a magnetic field, through the Lorentz force, significantly suppresses fluid motion and reduces convective heat transfer. As the influence of the magnetic field expands, both flow velocity and heat transfer decrease, demonstrating the magnetic field's effectiveness in controlling thermal and flow behavior within the cavity. Mirzaei et al. (2024b) numerically examined natural convection in a square porous cavity with a wavy cold vertical wall and a partial horizontal magnetic field applied to the hot wall. The study employed the Brinkman–Forchheimer-extended Darcy model and solved the governing equations using the finite element method. Results showed that the magnetic field suppresses heat transfer and fluid motion, while increasing the number of wall wave enhances thermal performance.

This study focuses on natural convection within a square porous cavity featuring a non-uniformly wavy wall and subjected to a partially applied magnetic field. The objective is to investigate heat transfer and fluid flow characteristics using numerical simulations and mathematical modeling. The findings contribute to existing knowledge by offering insights into how external influences such as magnetic fields and porous media affect natural convection behavior.

2. PROBLEM FORMULATION

This study considers laminar, incompressible natural convection within a cavity filled with porous material and subjected to a partially applied magnetic field. The configuration, illustrated in Figure 1, includes thermally insulated top and bottom walls, a heated left wall ($T = T_h$), and a wavy cold right wall ($T = T_c$). The cavity has a unit length and height ($L = H = 1$). The wavy right wall is defined by the parameters: $a = 1, b = 0.2, k' = 1$, and amplitude damping coefficient c. The porous medium is uniform, isotropic, and assumed to be in local thermal equilibrium with the fluid. Effects such as radiation, viscous dissipation, Joule heating, and induced magnetic fields are neglected in this analysis.

While Darcy's law provides a basic model for flow through porous media, it becomes inadequate in cases involving higher permeability, increased velocities, or larger Reynolds numbers. To address this, Forchheimer (1901) introduced a quadratic drag term to extend Darcy's law, accounting for inertial effects. Brinkman later enhanced the model by incorporating viscous forces for high-porosity media. Accordingly, this study adopts the Brinkman–Forchheimer-extended Darcy model to accurately represent the porous medium.

The flow within the cavity is modeled using the governing equations of continuity, momentum, and energy, formulated in terms of velocity components m(u, v), pressure (p), and temperature (T). These nonlinear equations capture the complex interactions of flow, thermal transport, and pressure distribution within the porous, magnetized cavity (Mirzaei et al., 2024b).

$$\nabla \cdot \mathbf{u} = 0 \tag{1}$$

$$\frac{\mu_e}{\rho_f \epsilon_p}\nabla^2 u = \frac{1}{\epsilon_p}\frac{\partial u}{\partial t} + \frac{1}{\epsilon_p^2}\left(u\frac{\partial u}{\partial x} + v\frac{\partial u}{\partial y}\right) + \frac{1}{\rho_f}\frac{\partial p}{\partial x} + \frac{\mu}{\rho_f \mathrm{K}}u + \frac{c_F}{\sqrt{\mathrm{K}}}|\mathbf{u}|u \tag{2}$$

$$\frac{\mu_e}{\rho_f \epsilon_p}\nabla^2 v = \frac{1}{\epsilon_p}\frac{\partial v}{\partial t} + \frac{1}{\epsilon_p^2}\left(u\frac{\partial v}{\partial x} + v\frac{\partial v}{\partial y}\right) + \frac{1}{\rho_f}\frac{\partial p}{\partial y} + \frac{\mu}{\rho_f \mathrm{K}}v + \frac{c_F}{\sqrt{\mathrm{K}}}|\mathbf{u}|v - g\beta(T - T_c) + \delta_B \frac{\sigma B_0^2}{\rho_f}v \tag{3}$$

$$\alpha_e \nabla^2 T = \sigma_h \frac{\partial T}{\partial t} + \mathbf{u} \cdot \nabla T \tag{4}$$

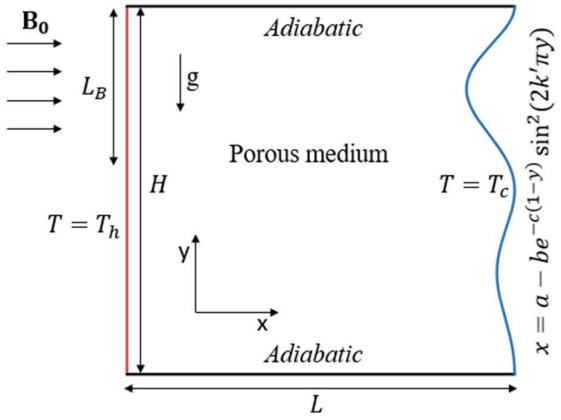

Figure 1: Definition of problem geometry.

In which μ corresponds to the dynamic viscosity of the fluid, the effective dynamic viscosity is μ_e, the fluid's density is ρ_f, the norm of the velocity vector $\sqrt{u^2+v^2}$ is $|\mathbf{u}|$, g is the gravitational acceleration, the thermal expansion coefficient is β, the pressure is defined by p, the porosity of a porous medium is measured by ϵ_p, the magnitude of the applied magnetic field is referred to as B_0, the fluid's electrical conductivity is defined as σ, the effective thermal diffusivity is $\alpha_e = \frac{k_e}{(\rho_f c_p)_f}$, the effective thermal conductivity is $k_e = \epsilon_p k_f + (1-\epsilon_p)k_s$, the specific heat at constant pressure is c_p, the coefficient of form is $c_F = \frac{1.75(1-\epsilon_p)}{d_p \epsilon_p^3}$, K $= \frac{d_p^2 \epsilon^3}{150(1 \quad p)^2}$ refers to permeability of the porous medium, d_p is the size of a solid particle in a porous medium, and the heat capacity ratio $\sigma_h = \frac{\epsilon_p(\rho_f c_p)_f + (1-\epsilon_p)(\rho_f c_p)_s}{(\rho_f c_p)_f}$, is considered one in this model. Additionally, the fluid (f) and solid (s) are assumed to have the same thermal conductivity and thermal diffusivity. That means, $k_e = k_f = k_s$ and $\alpha_e = \alpha_f = \alpha$. In addition, $\mu_e = \mu$ is assumed. Air fluid was used for the present work. The physical properties of air are given in Table 1.

The boundary conditions are outlined below:

$$u = v = 0, \frac{\partial T}{\partial y} = 0 \; at \; y = 0, 1, 0 < x < 1 \tag{5a}$$

$$u = v = 0, T = T_h \; at \; x = 0, 0 < y < 1 \tag{5b}$$

$$u = v = 0, T = T_c \; at \; x = a - be^{-c(1-y)} \; si\, n^2(2k'\pi y), 0 < y < 1 \tag{5c}$$

The dimensionless quantities are defined below:

$$X = \frac{x}{L}, Y = \frac{y}{L}, U = \frac{uL}{\alpha}, V = \frac{vL}{\alpha}, \tag{6a}$$

$$P = \frac{pL^2}{\rho_f \alpha^2}, t' = \frac{t\alpha}{L^2}, \theta = \frac{T - T_c}{T_h - T_c} \tag{6b}$$

With the help of non-dimensional quantities, they are replaced in the original Equations. (1) - (4), and assuming the elimination of prime symbols, the following dimensionless equations are obtained.

Table 1 Physical properties of air at 20℃.

Parameter	ρ_f	μ_f	c_p	k	σ
Physical Value	1.2047 kg/m^3	1.820×10^{-5} $kg/m.s$	1000 $J/kg.K$	0.02559 $W/m.K$	5×10^{-15}

$$\frac{\partial U}{\partial X}+\frac{\partial V}{\partial Y}=0 \tag{7}$$

$$\frac{Pr}{\epsilon_p}\nabla^2 U=\frac{1}{\epsilon_p}\frac{\partial U}{\partial t'}+\frac{1}{\epsilon_p^2}\left(U\frac{\partial U}{\partial X}+V\frac{\partial U}{\partial Y}\right)+\frac{\partial P}{\partial X}+\frac{Pr}{Da}U+\frac{c_g}{\sqrt{Da}}|\mathbf{u}|U \tag{8}$$

$$\frac{Pr}{\epsilon_p}\nabla^2 V=\frac{1}{\epsilon_p}\frac{\partial V}{\partial t'}+\frac{1}{\epsilon_p^2}\left(U\frac{\partial V}{\partial X}+V\frac{\partial V}{\partial Y}\right)+\frac{\partial P}{\partial Y}+\frac{Pr}{Da}V+\frac{c_g}{\sqrt{Da}}|\mathbf{u}|V-RaPr\theta+\delta_B Ha^2 Prv \tag{9}$$

$$\nabla^2\theta=\frac{\partial\theta}{\partial t}+U\frac{\partial\theta}{\partial x}+V\frac{\partial\theta}{\partial y} \tag{10}$$

where, $c_g=\frac{1.75}{\sqrt{150}\epsilon_p^{3/2}}$. The dimensionless parameters Prandtl, Darcy, Rayleigh, and Hartmann numbers are as follows:

$$Pr=\frac{\mu}{\alpha\rho_f}\,,Da=\frac{\mathrm{K}}{L^2}\,,Ra=\frac{g\beta\Delta T\rho_f L^3}{\mu\alpha}\,,Ha=B_0L\sqrt{\frac{\sigma}{\mu}} \tag{11}$$

where $\Delta T=T_h-T_c$. By setting the stream function ψ as $u=\frac{\partial\psi}{\partial y},v=-\frac{\partial\psi}{\partial x}$, it eliminates the continuity equation due to satisfying the continuity condition, and the pressure term is removed by using the vorticity definition $\omega=\nabla\times\mathbf{u}$ in the momentum equation equations. Non-dimension equations are deduced from the effects of stream and vorticity functions:

$$\nabla^2\psi=\omega \tag{12}$$

$$\nabla^2\omega=\frac{1}{Pr}\frac{\partial\omega}{\partial t'}+\frac{1}{Pr\epsilon_p}\left(U\frac{\partial\omega}{\partial X}+V\frac{\partial\omega}{\partial Y}\right)+\frac{\epsilon_p}{Da}\omega+\frac{c_g\epsilon_p}{Pr\sqrt{Da}}\left[V\frac{\partial|\mathbf{u}|}{\partial X}-U\frac{\partial|\mathbf{u}|}{\partial Y}+|\mathbf{u}|\omega\right]-\epsilon_p Ra\frac{\partial\theta}{\partial X}+\epsilon\delta_B Ha^2\frac{\partial V}{\partial X} \tag{13}$$

$$\nabla^2\theta=\frac{\partial\theta}{\partial t}+U\frac{\partial\theta}{\partial x}+V\frac{\partial\theta}{\partial y} \tag{14}$$

In the case of the incoming magnetic field, δ_B , is defined as:

$$\delta_B=\begin{cases}0, 0\le y<1-L_B\\ 1, 1-L_B\le y<1\end{cases} \tag{15}$$

The reduced boundary conditions are as follows:

$$\psi=0,\frac{\partial\theta}{\partial Y}=0\ at\ y=0,1,0<X<1 \tag{16a}$$

$$\psi=0,\theta=1\ at\ X=0,0<Y<1 \tag{16b}$$

$$\psi=0,\theta=0\ at\ X=a-be^{-c(1-Y)}\ sin^2(2k'\pi Y)\,,0<Y<1 \tag{16c}$$

The average Nusselt number for the warm wall is determined as follows:

$$\overline{Nu}=\int_0^1-\frac{\partial\theta}{\partial X}dY \tag{17}$$

3. METHOD OF SOLUTION

Equations (12) - (14) are solved using the Galerkin Finite Element Method (FEM) along with the boundary conditions specified in Equation (16). FEM is chosen for its robustness and flexibility in handling complex problems. Once the initial mesh is generated, the solution progresses iteratively, with adaptive adjustments to the mesh structure if necessary to improve accuracy. This iterative process continues until the convergence criterion of 10^{-5} is satisfied.

The core principle of FEM involves discretizing a complex domain into smaller sub-regions known as finite elements. Each element has a defined geometry and is described mathematically through equations that model the system's behavior locally. Shape functions are employed to interpolate the solution within each element using nodal values. In this work, FEM is applied to numerically solve the governing equations for natural convection within a square, non-uniform wavy cavity filled with porous media and influenced by a partial magnetic field. Figure 2 illustrates the numerical procedure, while Figure 3 demonstrates strong agreement between the obtained streamlines and isotherms and those reported by Mirzaei et al. (2024b). Table 2 represents the quantitative data average Nusselt number comparison between present work and Mirzaei et al. (2024b).

To ensure mesh-independent results, a grid independence study was conducted. The test case involved natural convection in a cavity with a damped sine wave profile on one side and a magnetic field applied to part of that boundary. Four different mesh densities were tested, and as shown in Table 3, the solution stabilized with 2427 cells, achieving the required accuracy of 10^{-5}. The optimized mesh configuration is presented in Figure 4.

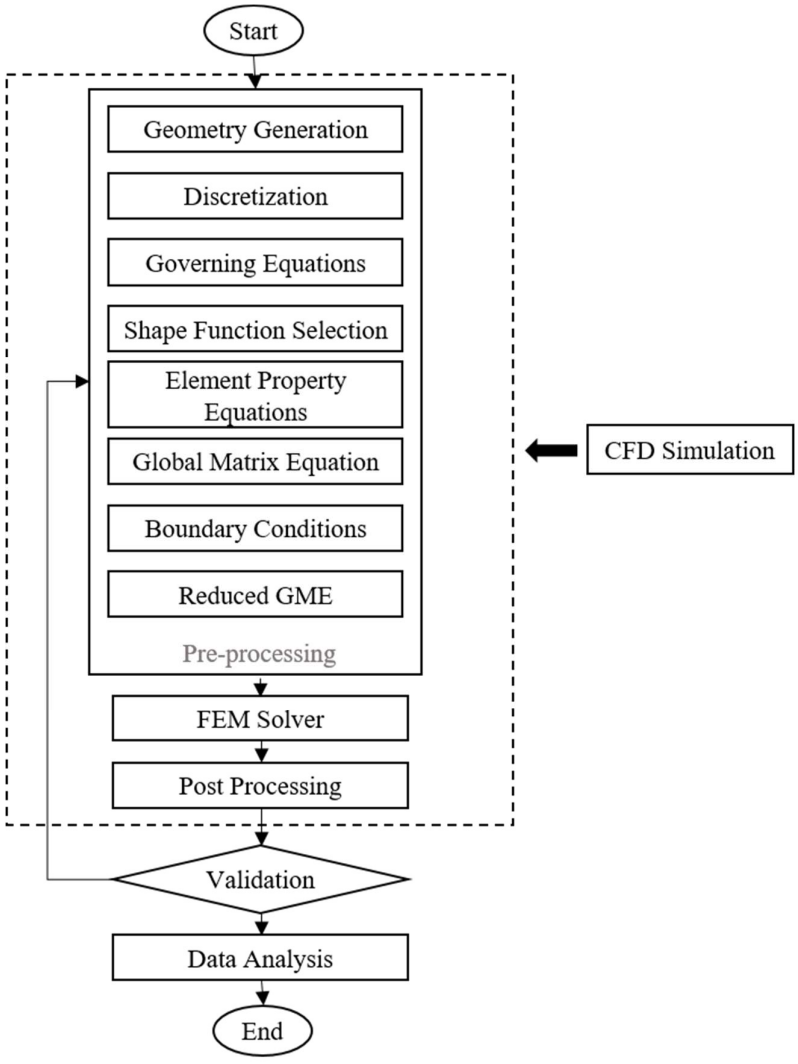

Figure 2: The flowchart of the numerical method.

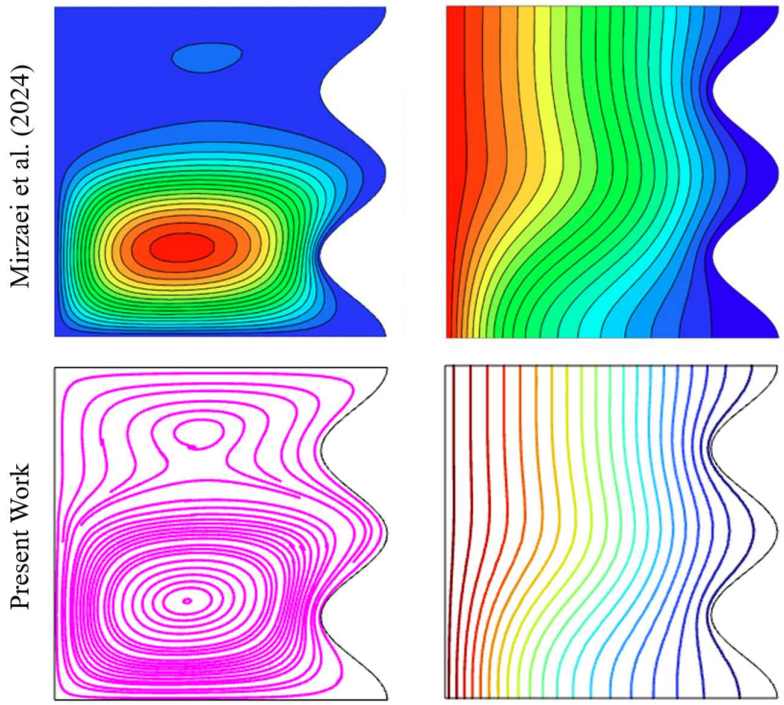

Figure 3: Comparison of streamlines (on the left) and isotherm lines (on the right) at Ra = 10^4, Da = 0.01, ϵ_p = 0.9, Ha = 100, LB = 0.5, $k' = 2$.

Table 2 Quantitative result comparison.

	Mirzaei et al. (2024)	Present Work
$\overline{Nu}$	1.465	1.313

Table 3 Mesh independent review with $Ra = 10^5, Da = 0.01, \epsilon_p = 0.9, Ha = 50, L_B = 0.5, c = 2$.

Elements	1027	1481	2427	6514
$\overline{Nu}$	3.0841	3.0723	3.0514	3.0141

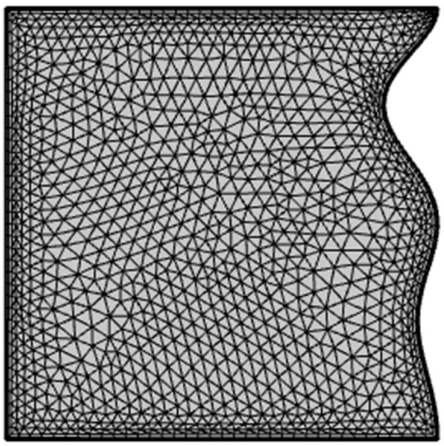

Figure 4: Grid of geometry.

4. RESULTS AND DISCUSSIONS

Figure 5 illustrates the effect of increasing the length of the applied magnetic field along the left wall. As the magnetic field lengthens, the primary vortex shifts downward and becomes confined to the lower-left corner of the cavity, while its upper section is stretched toward the upper-right corner. This distortion results from the expanding region influenced by the Lorentz force. As the magnetic field length increases, the vortex weakens, and buoyancy-driven flow slows. This leads to a reduction in temperature gradients, with isotherms appearing more flattened, signifying the magnetic field's suppressive effect on natural convection.

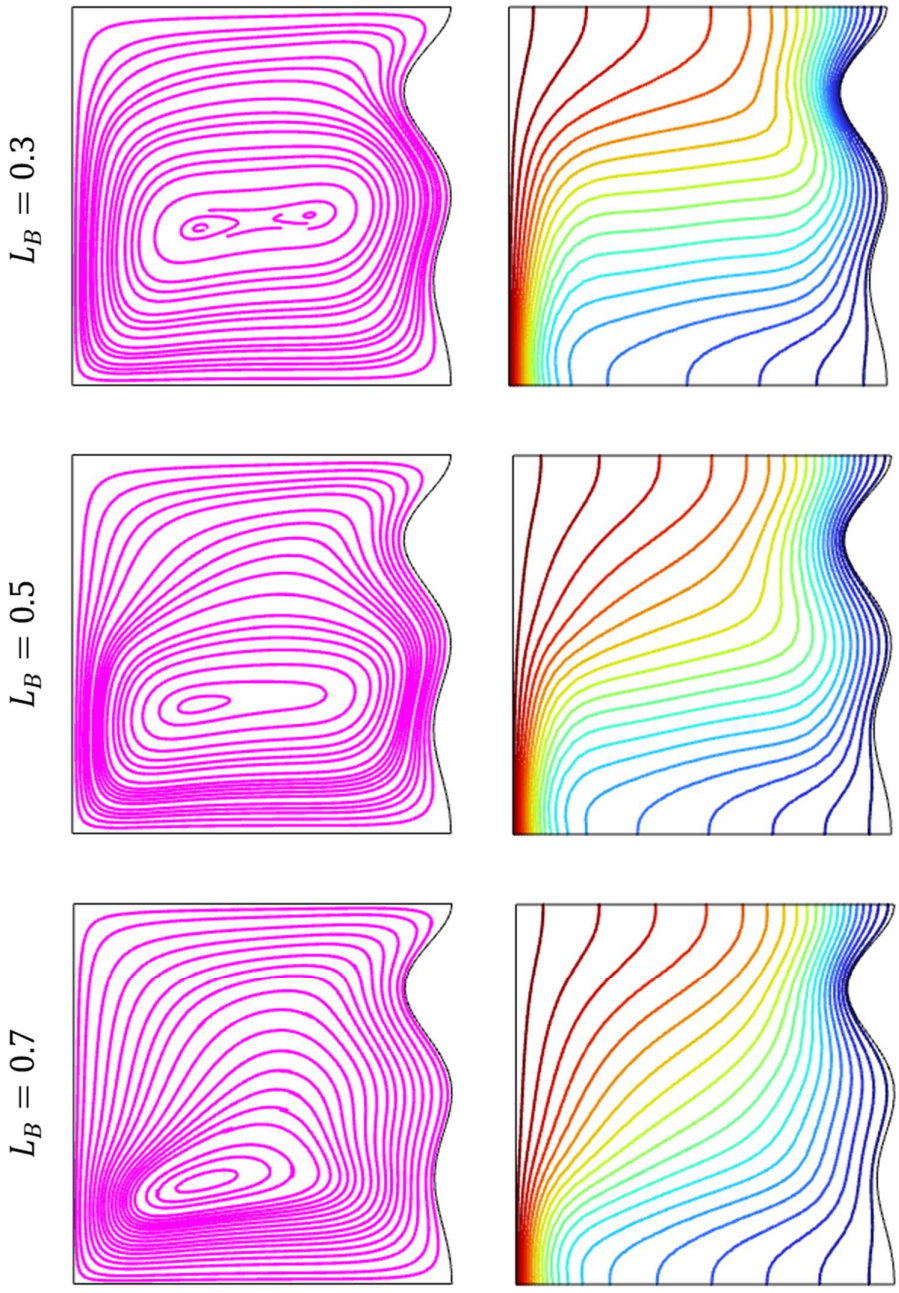

Figure 5: Impact of magnetic field length on streamlines and isotherm lines with $Ra = 10^5, Da = 0.01, \epsilon_p = 0.9, Ha = 50, c = 2$; from top to bottom Nu = 3.6264, 3.0514, 2.44, respectively.

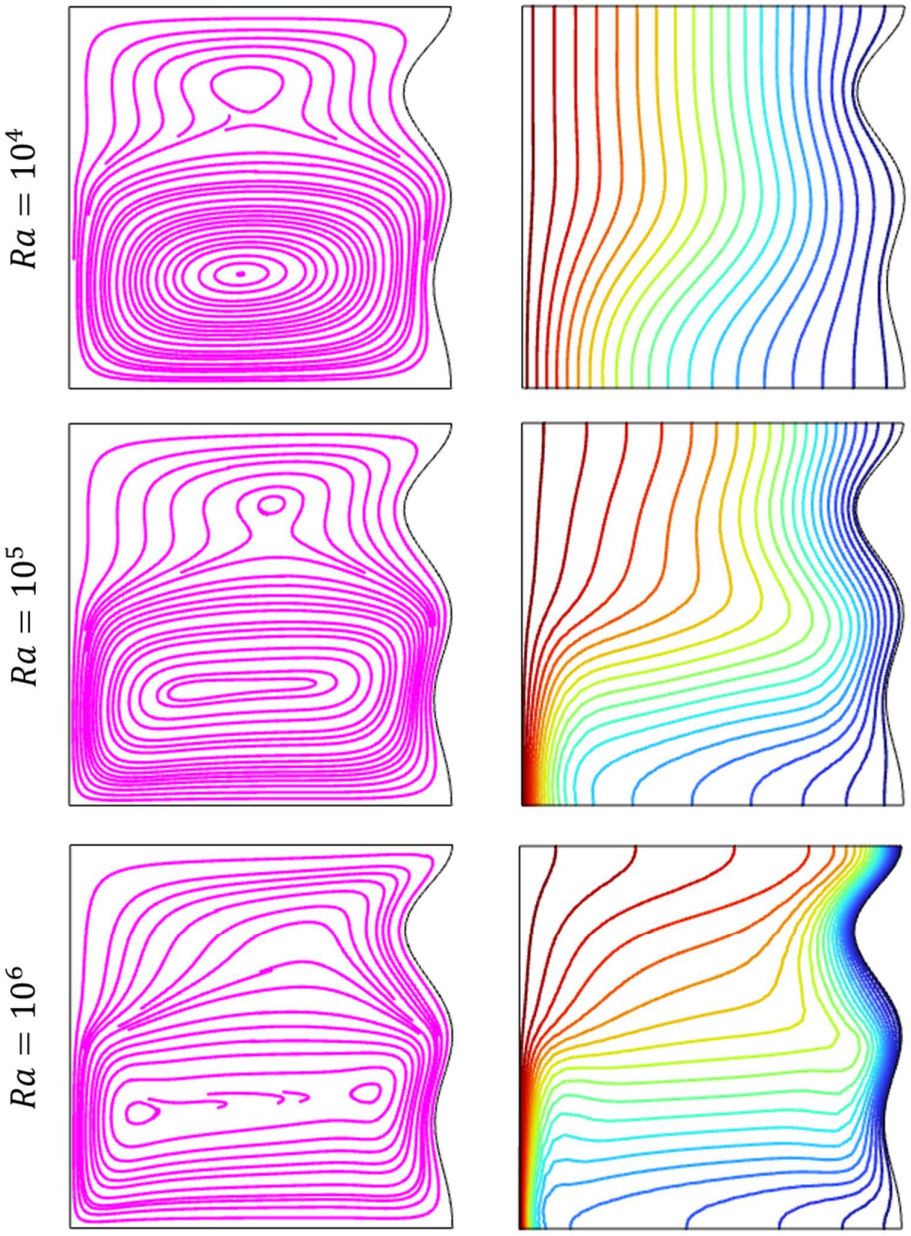

Figure 6: Influence of Rayleigh number on streamlines and isotherm lines with $Da = 0.01, \epsilon_p = 0.9, Ha = 100, L_B = 0.5, c = 2$; from top to bottom Nu = 1.1975, 2.5667, 6.333, respectively.

Figure 6 presents the influence of the Rayleigh number on streamlines and isotherms, with $L_B = 0.5$ indicating that the magnetic field acts from the top to the center of the left wall. In this configuration, streamlines reflect natural convection at the bottom of the cavity, while the upper part shows the delayed effect of the Lorentz force. At $Ra = 10^4$, a secondary vortex forms due to Lorentz force dominance over buoyancy. However, at higher Rayleigh numbers (10^5 and 10^6), stronger buoyancy forces suppress the secondary vortex. The isotherms appear nearly perpendicular to the top wall at $Ra = 10^4$ and 10^5, and as Rayleigh increases, they bend more, indicating deeper heat penetration into the cavity's upper region.

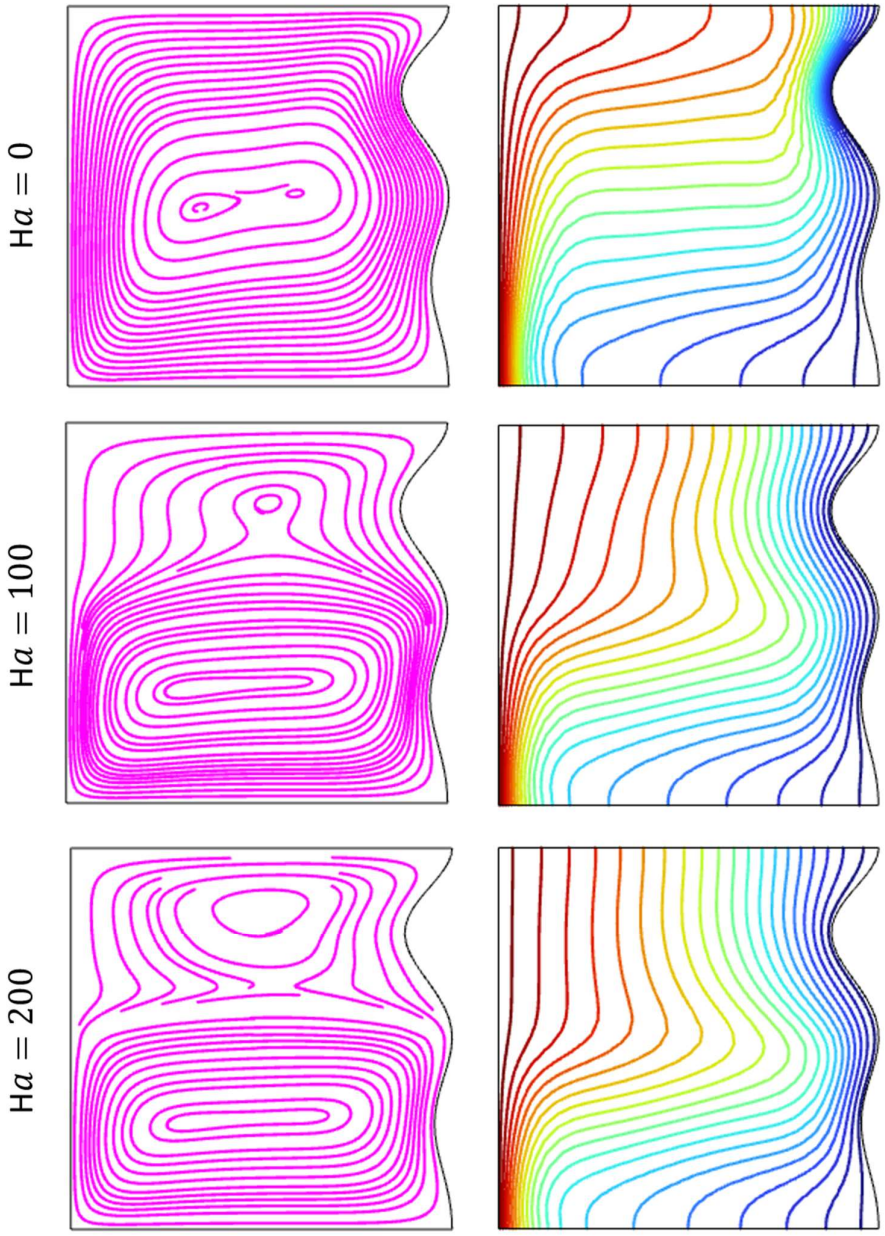

Figure 7: Impact of Hartmann number on streamlines and isotherm lines with $Da = 0.01, \epsilon_p = 0.9, Ra = 10^5, L_B = 0.5, c = 2$; from top to bottom Nu = 4.02, 2.5667, 2.3774, respectively.

Figure 7 explores the impact of the Hartmann number on flow and temperature distribution. In the absence of a magnetic field (i.e., no Lorentz force), streamlines reflect natural convection throughout the cavity. As the Hartmann number increases, the vortex shifts downward and weakens. Isotherms, especially for $Ra = 10^5$ and 10^6, become more vertical near the top wall, and with increasing Rayleigh number, their curvature decreases, demonstrating that the magnetic field increasingly controls both heat transfer and flow dynamics.

Figure 8 shows the effect of the Darcy number on streamlines and isotherms. At low Darcy values, vortex formation is centered, and isotherms appear nearly parallel, indicating weak fluid motion and diminished Lorentz force influence. As the Darcy number increases, fluid velocity rises, enhancing heat penetration and shifting the vortex downward.

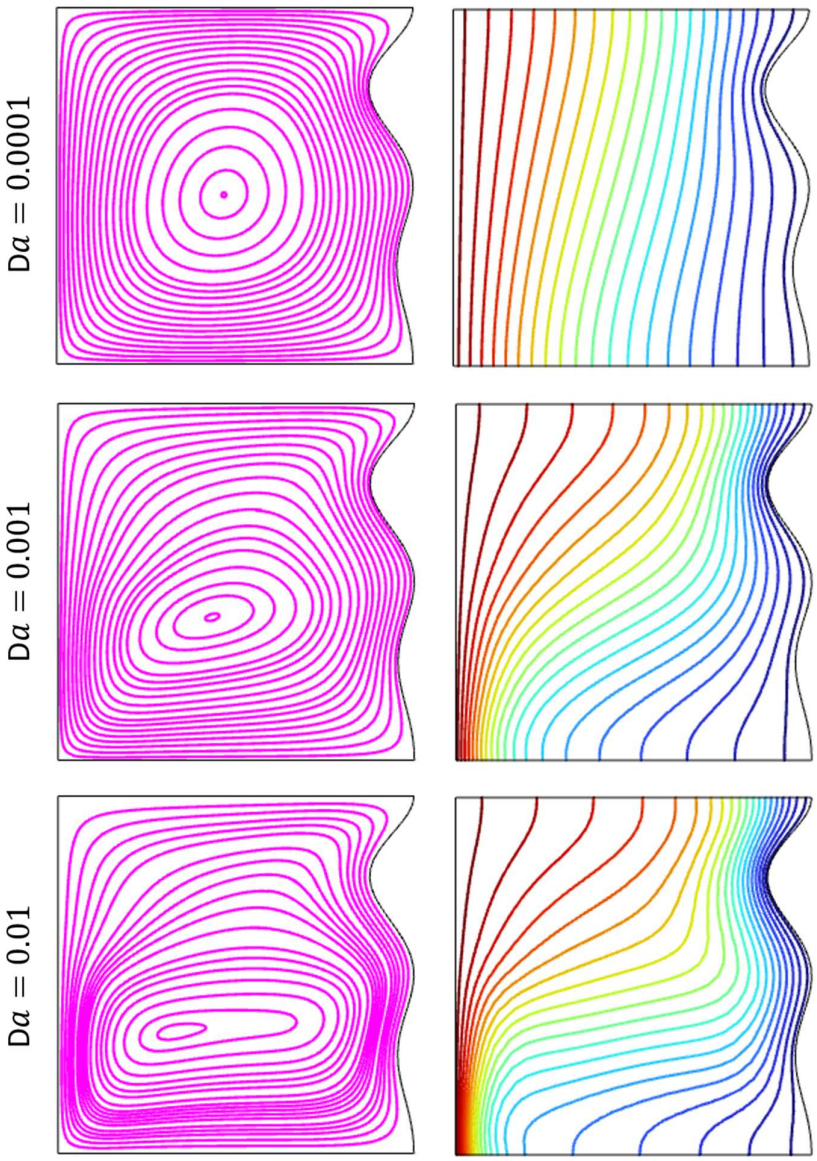

Figure 8: Impact of Darcy number on streamlines and isotherm lines with $Ra = 10^5, \epsilon_p = 0.9, Ha = 50, L_B = 0.5, c = 2$; from top to bottom Nu = 1.1233, 2.02, 3.0514, respectively.

Figure 9 examines the damping effect of wall wave on flow and thermal fields. With higher wave damping effect. The wave number has minimal effect on the isotherms; however, it does contribute to a slight decreas in the average Nusselt number, indicating reduced convective heat transfer.

Finally, Figure 10 illustrates how average Nusselt number varies with magnetic field length, Rayleigh number, Hartmann number, and Darcy number. Heat transfer improves with increasing Rayleigh and Darcy numbers, while higher Hartmann numbers and longer magnetic field lengths reduce the average Nusselt number. This demonstrates that thermal performance can be enhanced or suppressed depending on the interplay between buoyancy, porous resistance, and magnetic forces.

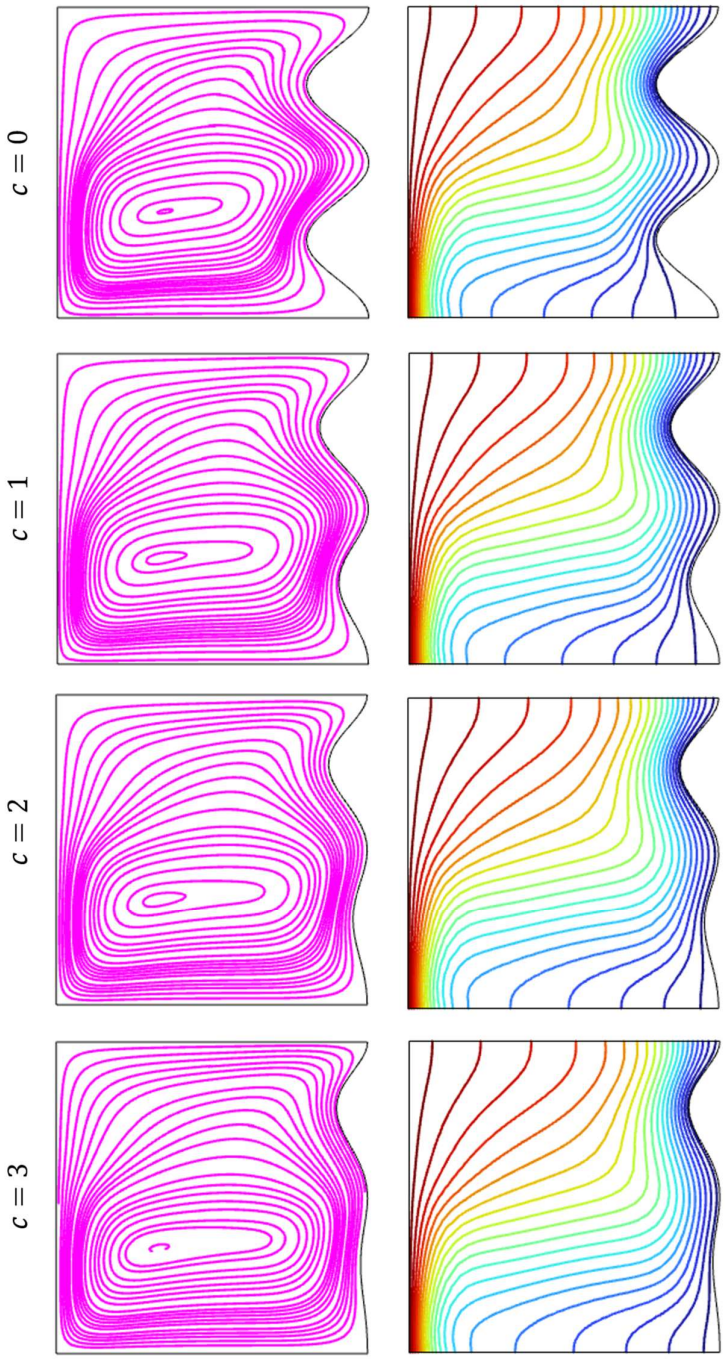

Figure 9: Impact of wave number on streamlines and isotherm lines with $Ra = 10^5, Da = 0.01, \epsilon_p = 0.9, Ha = 50, L_B = 0.5$; from top to bottom Nu = 3.1342, 3.0814, 3.0514, 3.0337, respectively.

4. CONCLUSION

This study numerically analyzed natural convection within a square wavy porous cavity under the influence of a partially applied magnetic field. Key parameters—including magnetic field length (L_B), Rayleigh number (Ra), Hartman number (Ha), Darcy number (Da), and wave damping effect (c) were varied within the ranges $L_B = 0.3 - 0.7, Ra = 10^4 - 10^6, Da = 0.0001 - 0.01,$ and $c = 1 - 3$. The simulations evaluated the effects of these parameters on temperature distribution, average Nusselt number, streamlines, and isotherms. The main findings are summarized below:

1. **Magnetic field length**: Increasing the length of the applied magnetic field reduces heat transfer. Specifically, as L_B increases from 0.3 to 0.7, the average Nusselt number drops by 36.6%.
2. **Rayleigh number**: Higher Ra values enhance heat transfer and fluid motion due to stronger buoyancy forces. An increase in R_a from 10^4 to 10^6 results in more than a fivefold increase in the Nusselt number.
3. **Secondary vortex formation**: At lower Rayleigh numbers, a secondary vortex appears, caused by the Lorentz force dominating over buoyancy.
4. **Lorentz force impact**: The suppressive effect of the Lorentz force on heat transfer and fluid flow becomes more pronounced at higher Rayleigh numbers.
5. **Hartmann number**: As Ha increases, the Lorentz force intensifies, leading to a reduction in both heat transfer and flow strength. A rise in Ha from 0 to 200 decreases the Nusselt number by 44%.
6. **Darcy number**: Enhanced permeability in the porous medium significantly improves heat transfer. As Da increases from 0.0001 to 0.01, the Nusselt number more than doubles.
7. **Effectiveness of magnetic field**: At low Darcy numbers, the magnetic field has minimal impact due to weak fluid motion.
8. **Wave damping effect**: The increasing damping effect in the wave function results in reduced Nusselt number. Which validates that more curvature means more area for heat transfer therefore resulting Nusselt number is higher.

REFERENCES

1. Pandey, S., Park, Y. G., & Ha, M. Y. (2019). An exhaustive review of studies on natural convection in enclosures with and without internal bodies of various shapes. *International Journal of Heat and Mass Transfer*, *138*, 762–795. https://doi.org/10.1016/j.ijheatmasstransfer.2019.04.097
2. Rahimi, A., Saee, A. D., Kasaeipoor, A., & Malekshah, E. H. (2018). A comprehensive review on natural convection flow and heat transfer. *International Journal of Numerical Methods for Heat &Amp Fluid Flow*, *29*(3), 834–877. https://doi.org/10.1108/hff-06-2018-0272
3. Parmar, D., Kumar, B. V. R., Murthy, S. V. S. S. N. V. G. K., & Kumar, S. (2023). Numerical study of entropy generation in magneto-convective flow of nanofluid in porous enclosure using fractional order non-Darcian model. *Physics of Fluids*, *35*(9). https://doi.org/10.1063/5.0169204
4. Rath, C., & Nayak, A. (2023). A numerical study on MHD Cu-Al2O3/H2O hybrid nanofluid with Hall current and cross-diffusion effect. *Physics of Fluids*, *35*(10). https://doi.org/10.1063/5.0169236
5. Davidson, P. A. (2001). *An Introduction to Magnetohydrodynamics*. https://doi.org/10.1017/cbo9780511626333
6. Wu, D., Lai, Y., & Zhang, M. (2015). Heat and mass transfer effects of ice growth mechanisms in a fully saturated soil. *International Journal of Heat and Mass Transfer*, *86*, 699–709. https://doi.org/10.1016/j.ijheatmasstransfer.2015.03.044
7. Tuli, S. S., Saha, L. K., & Roy, N. C. (2023). Effect of inclined magnetic field on natural convection and entropy generation of non-Newtonian ferrofluid in a square cavity having a heated wavy cylinder. *Journal of Engineering Mathematics*, *141*(1). https://doi.org/10.1007/s10665-023-10279-2
8. Kolsi, L., Rashad, A., Biswas, N., Mansour, M., Salah, T., Eladeb, A., & Armaghani, T. (2024). Radiation and heat generation effect on MHD natural convection in hybrid nanofluid-filled inclined wavy porous cavity incorporating a cross-shaped obstacle. *International Journal of Numerical Methods for Heat &Amp Fluid Flow*. https://doi.org/10.1108/hff-07-2024-0556
9. Hasan, N., Deb, N., & Saha, S. (2024). MHD Convection with Joule Heating and Internal Heat Generation in a Two-Layer Discretely Heated Chamber Partly Filled with Porous Medium. *International Journal of Energy Research*, *2024*(1). https://doi.org/10.1155/2024/1720993
10. Halder, A., Bhattacharya, A., Biswas, N., Manna, N. K., & Mandal, D. K. (2024). MHD nanofluidic mixed convection and entropy generation in a butterfly-shaped cavity. *Sadhana*, *49*(1). https://doi.org/10.1007/s12046-024-02428-9
11. Barman, P., & Rao, P. S. (2023). Numerical analysis of local thermal non-equilibrium free convection in a porous enclosure with a wavy cold side wall. *Proceedings of the Institution of Mechanical Engineers Part E Journal of Process Mechanical Engineering*, *238*(1), 372–382. https://doi.org/10.1177/09544089231154363
12. Geridonmez, B. P., & Oztop, H. (2020). MHD natural convection in a cavity in the presence of cross partial magnetic fields and Al2O3-water nanofluid. *Computers & Mathematics With Applications*, *80*(12), 2796–2810. https://doi.org/10.1016/j.camwa.2020.10.003
13. Geridonmez, B. P., & Oztop, H. F. (2019). Natural convection in a cavity filled with porous medium under the effect of a partial magnetic field. *International Journal of Mechanical Sciences*, *161–162*, 105077. https://doi.org/10.1016/j.ijmecsci.2019.105077
14. Geridonmez, B. P., & Oztop, H. F. (2020b). Natural convection in a cavity under partial magnetic field applied from different corners. *International Communications in Heat and Mass Transfer*, *114*, 104575. https://doi.org/10.1016/j.icheatmasstransfer.2020.104575
15. Mirzaei, A., Jalili, B., Jalili, P., & Ganji, D. D. (2024b). Free convection in a square wavy porous cavity with partly magnetic field: a numerical investigation. *Scientific Reports*, *14*(1). https://doi.org/10.1038/s41598-024-64850-7